Chemical Physics Letters 481 (2009) 204–208

Contents lists available at ScienceDirect

Chemical Physics Letters

journal homepage: www.elsevier.com/locate/cplett

Real-time observation of dynamic coupling between the stretching and bending modes in a polythiophene

Juan Du [a,b], Takayoshi Kobayashi [a,b,c,d,*]

[a] Department of Applied Physics and Chemistry and Institute of Laser Science, University of Electro-Communications, Chofugaoka 1-5-1, Chofu, Tokyo 182-8585, Japan
[b] JST, ICORP, Ultrashort Pulse Laser Project, 4-1-8 Honcho, Kawaguchi, Saitama 332-0012, Japan
[c] Department of Electrophysics, National Chiao Tung University, 1001 Ta Hsueh Road, Hsin-chu 3005, Taiwan
[d] Institute of Laser Engineering, Osaka University, 2-6 Yamada-Oka, Suita 565-0871, Japan

ARTICLE INFO

Article history:
Received 7 July 2009
In final form 25 September 2009
Available online 30 September 2009

ABSTRACT

By real-time vibrational spectroscopy using 6.3 fs pulses, both instantaneous frequency and amplitude modulated with frequency of 120–130 cm^{-1} were observed for the C–C stretching mode with the central frequency of 1343 cm^{-1} in a poly-(substituted thiophene). This provided the evidence that a stretching mode dynamically couples with another stretching mode mediated by a low-frequency bending mode. Instantaneous bond-order changed during the bending motion due to the change in the distribution of π-electrons. The coupling between the stretching and bending modes was found to be maintained for longer than 1200 fs after the start of the coherent molecular vibration.

1. Introduction

It is now widely recognized that polythiophenes (PTs) have a significant potential in the development of electronic devices such as field-effect transistors [1], solar cells [2], batteries, and diodes. This has become possible thanks to their electrical conductivity, which is the most notable property of PTs and results from the delocalization of electrons along the polymer backbone. Beside the conductivity, color change is another interesting property resulting from change in the degree of electron delocalization. Dramatic spectral shifts will be observed if the environmental stimulus changes, such as temperature [3–6] and the solvent [3–5,7]. Both changes in color and conductivity make the conjugated polymers attractive for various devices in optoelectronics such as nonlinear optic devices [8] and chemical sensors [9].

Because of the significant attention paid to PTs over the last three decades, a detailed understanding of the dynamics of photoexcitations in them and their derivatives are highly desirable for practical reasons. Coherent vibrations in molecules are well formulated by time-dependent wavepacket description. Based on this, one can build up theoretical models for geometrical changes according to experimental results. The amplitude of molecular vibration can be probed through a change in electronic transition probability. The vibrational dynamics then can be studied from the change in the electronic transition probability and/or electronic spectral shape induced by femtosecond lasers, whose pulse duration is shorter than the vibrational periods. The time-dependent energy redistribution among the modes through mode coupling can be clarified. However, in the case of conjugated polymer systems, there is a well-known problem that most of their morphology is amorphous. This means that the electronic states of such amorphous polymers are highly inhomogeneous due to relatively broad distributions of chain lengths, conjugation lengths, and degrees of interaction strength between neighboring chains. Thus the relaxation dynamics of electronic states could be very complicated due to the different dynamic in the inhomogeneous surrounding. It is useful to study the dynamics of electronic state and vibrational modes simultaneously, since they are correlated through vibronic coupling. Therefore, simultaneous measurement of electronic and vibrational dynamics in a broad spectral range is desirable to study dynamics in conjugated polymers.

The methodology used in the present study is femtosecond pump–probe real-time vibration spectroscopy. Compared with other vibrational spectroscopies, such as infrared absorption and Raman scattering, it has many advantages. They have (1) the possibility of simultaneous investigation on electronic relaxation processes and the dynamics of vibrational modes coupled to the electronic transition, (2) the possibility of measurement of low-frequency, (3) ability of vibrational phase detection, and (4) direct observation of vibronic dynamics including time-dependent instantaneous frequencies.

In the present Letter, we applied this method to a polymer of thiophene derivative, PHTDMABQ, which belongs to a quinoid–benzenoid polythiophene. This is a kind of low band-gap polymers,

* Corresponding author. Address: Department of Applied Physics and Chemistry and Institute of Laser Science, University of Electro-Communications, Chofugaoka 1-5-1, Chofu, Tokyo 182-8585, Japan. Fax: +81 42 443 5825.
E-mail addresses: dujuan@ils.uec.ac.jp (J. Du), kobayashi@ils.uec.ac.jp (T. Kobayashi).

0009-2614/$ - see front matter © 2009 Elsevier B.V. All rights reserved.
doi:10.1016/j.cplett.2009.09.091

and those polymers have been a focus of research on new nonlinear optical (NLO) materials because of their often ultrafast large third-order NLO susceptibility and inherent chemical design flexibility [10,11]. In spite of the unique feature of this polymer originating from the coexisting benzenoid and quinoid rings, ultrafast dynamics of the electronic structure of the polymer has never been well studied except in our recent Letter on the excited state phase dynamics by the method of 'negative time' [12]. It was found that the instantaneous vibrational frequency and amplitude of C–C stretching mode with average frequency of 1343 cm^{-1} were modulated by the bending mode with 120–130 cm^{-1}. This finding led to the conclusion that the bending mode dynamically couples with the C–C stretching mode through instantaneous bond-order change during the bending motion.

2. Experimental

The sample used in the present study is a newly synthesized quinoid–benzenoid polythiophene, poly{[3-hexylthiophene-2,5-diyl]-[p-dimethylaminobenzylidenequinoidmethene]} (PHTDMABQ), which was provided by Profs. Katsumi Yoshino and Wei Feng. It was dissolved in methanol and cast on a quartz substrate for the measurement of stationary and time-resolved spectra.

A noncollinear optical parametric amplifier (NOPA) seeded by a white-light continuum was used as a light source of both the pump and probe pulses, as described in Refs. [13–16]. The pump source of this NOPA system is a commercially supplied regenerative amplifier (Spectra Physics, Spitfire), whose central wavelength, pulse duration, repetition rate, and average output power were 800 nm, 50 fs, 5 kHz, and 650 mW, respectively. The output of NOPA covered the spectral range extending from 515 to 716 nm, and its pulse duration was compressed to 6.3 fs using a system composed of a pair of Brewster-angle prisms with an apex angle of 68° and chirp mirrors (Layertec). The pulse energies of the pump and probe were typically about 50 and 6 nJ, respectively.

In the present experiment, we applied the combination of polychromator and multichannel lock-in amplifier to detect the pump–probe signal. The reference and probe pulses were dispersed by the polychromator (300 groove/mm, 500 nm blazed) and simultaneously guided to the photodetector by a 128-channel bundle fiber. The spectral resolution of the total system, which is composed of the monochromator, a bundle fiber, and an arrayed system of photodetectors, was ~1.5 nm. The pump–probe experiment of the PHTDMABQ film sample was measured for 128 wavelengths with a probe-delay time from −200 to 1800 fs, and a constant delay time step was set to be 0.2 fs. All of the experiments were performed at room temperature (293 ± 1 K).

3. Results and discussion

3.1. Fourier analysis of real-time vibrational traces

The stationary absorption and the fluorescence spectra of PHTDMABQ were measured with an absorption spectrometer (Shimadzu, UV-3101PC) and a fluorophotometer (Hitachi, F-4500), respectively. Fig. 1 shows the stationary spectra, the molecular structure, and the output spectrum of the 6.3 fs NOPA laser.

Fig. 2a depicts eight examples of the real-time traces of the difference absorbance out of 128 traces as a function of the pump–probe-delay time at various probe wavelengths. The signals of finite size at negative delay times are due to the perturbed free-induction decay associated with the third-order nonlinear vibronic polarization generated by the sequential interaction of probe–pump–pump fields. The sharp and intense peaks around zero probe-delay time are due to pump–probe coupling induced by

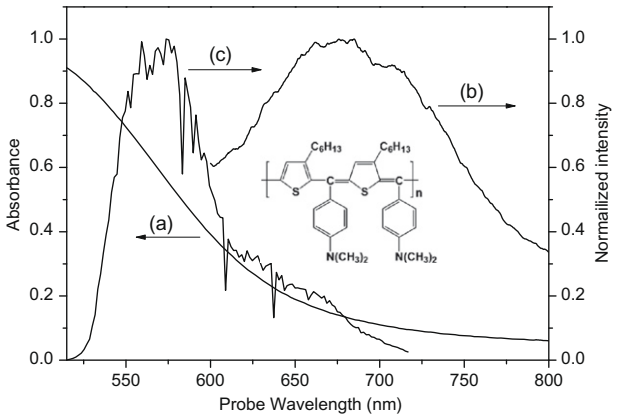

Fig. 1. Electronic spectra of PHTDMABQ and laser spectrum: (a) stationary absorption spectrum, (b) fluorescence spectrum, and (c) the output spectrum of the 6.3 fs NOPA laser. The inset is the structure of molecule studied.

the nonlinear process of the pump–probe–pump time-ordering interaction of the fields and the interference between the scattered pump pulses and the probe pulses.

It is obvious that the signals shown in Fig. 2a are composed of slow dynamics and oscillating components, which we ascribe to the electronic and vibrational dynamics, respectively. The oscillatory signals extend up to ~500 fs, and the Fourier transform (FT) analysis results of these oscillatory signals are shown in Fig. 2b. This FT analysis was performed after averaging over 200 fs to remove the slow decay dynamics due to dynamics in the relevant electronic states. The real-time data ranging from 0 to 100 fs were not included in the calculation of FT spectra to avoid the possible interference effects between the scattered pump and probe pulses. There is one predominant peak at 1343 cm^{-1} and three other small peaks located at 1111, 1192, and 1465 cm^{-1}. The phases of these modes calculated at all the probe wavelengths were neither 0 (or $\pm\pi$) nor $\pm\pi/2$. It means that the wavepackets in both ground and excited states contribute to these signals.

3.2. Spectrogram analysis of time-dependent frequencies and amplitudes

In order to discuss the dynamics of the interaction among the modes, a spectrogram analysis was performed with a Blackman window function using an FWHM of 160 fs to study the gate delay time-dependent instantaneous frequencies and amplitudes of several modes. Two dimensional displays of the spectrograms at 635 and 650 nm, plotted in Fig. 3, clearly exhibit the features of both frequency and intensity modulations for the 1343 cm^{-1} mode.

The Fourier power spectra of the modulation traces of frequency and integrated amplitude have peak frequencies of 122 and 130 cm^{-1}, respectively, as shown in Fig. 4. The two modulation frequencies agree with each other within the experimental error due to limited time range of the measurement. Both of them are close to the difference between the Fourier power peaks at 1465 and 1343 cm^{-1}. Therefore, one could argue that the observed frequency and intensity modulation could in principle be attributed to the artifact, which is caused by the coupling between the 1465 and 1343 cm^{-1} in the spectrogram calculation, though the intensity of 1465 cm^{-1} is much weaker than that of 1343 cm^{-1}.

It was verified by comparison of the experimental results with model calculations that neither frequency nor amplitude modulations are induced by artificial interference due to the finite spectral resolution associated with the time-gate width. The effect of the artifact could be simulated by calculating the spectrogram of a

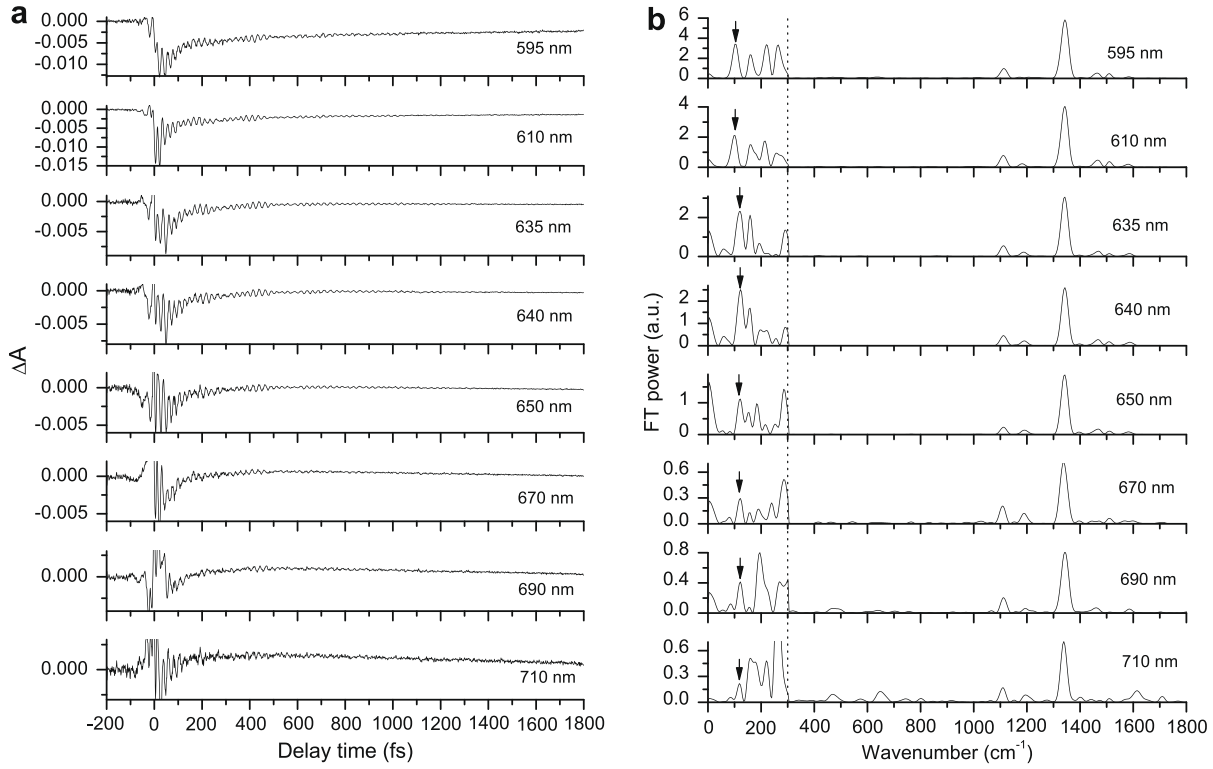

Fig. 2. Real-time vibrational spectra and the corresponding FT power spectra of the vibrations at the same probe wavelengths: (a) changes in the absorbance as functions of pump–probe-delay time and (b) the FT power spectra of real-time vibrational spectra (the intensity in the range of 0–300 cm^{-1} is expanded by 60 times).

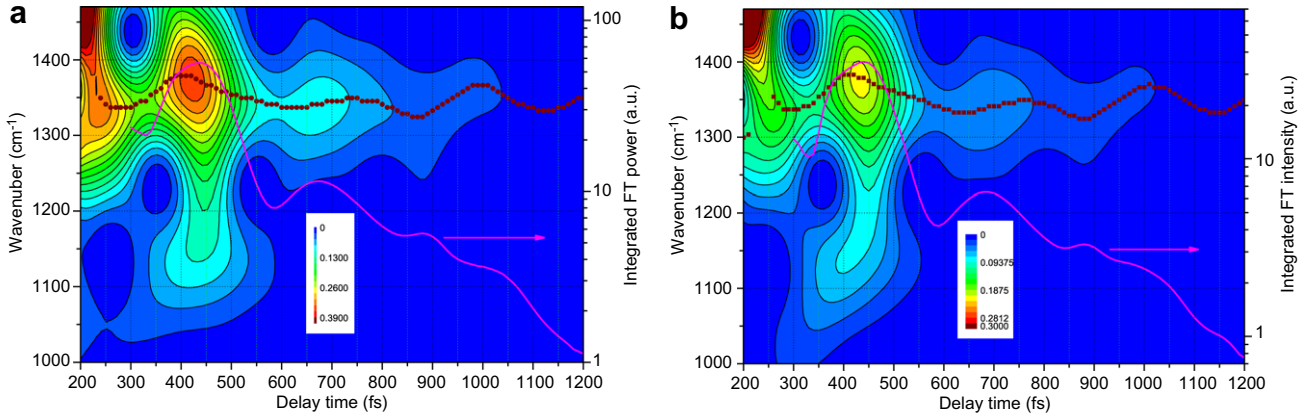

Fig. 3. Contour maps of the two-dimension Fourier powers of vibrational components obtained by spectrogram calculation for the real-time data calculated for the real-time vibrational traces probed at (a) 635 nm and (b) 650 nm. The dotted and solid lines denote the frequency and integrated intensity modulations, respectively.

model, which is a linear combination of two functions representing the corresponding two modes:

$$y_i(t) = A_e \exp(-t/\tau_e) + B_{vi} \exp(-t/\tau_{vi} \cos(\omega_i t + \phi_i), \quad (i = 1, 2). \tag{1}$$

Here, ω_1 and ω_2 are the angular frequencies corresponding to the wavenumbers of 1343 and 1465 cm^{-1}; τ_e is the electronic decay time; τ_{v1} (260 fs) and τ_{v2} (228 fs) are the vibration decay times determined from the FWHW of the Fourier power spectra of the modes with frequencies of ω_1 and ω_2; φ_1 (0.59π) and φ_2 (-0.53π) are the initial phases of ω_1 and ω_2 modes at 635 nm, respectively. B_{v1} and B_{v2} are the vibrational amplitudes of ω_1 and ω_2, and the ratio between them is calculated to be 3.8:1.

Using the same Blackman window (FWHM of 160 fs) as that used for the experimental data analysis, the results of simulation shown in Fig. 5a were obtained. The modulations in wavenumbers and integrated amplitudes calculated from the spectrogram for the simulation (Fig. 5a) compared with those of the experimental results are shown in Fig. 5b and c, respectively. As shown in Fig. 5b, the frequency modulation strength induced by the artificial interference is much smaller than that of the experimental observation. Furthermore, a similar feature is observed in the strength of the integrated amplitude modulation. Therefore, because of the two neighboring vibrational modes, the artificial interference due to the mathematical expansion of the spectral width induced by the finite width of the window has an appreciable effect on the

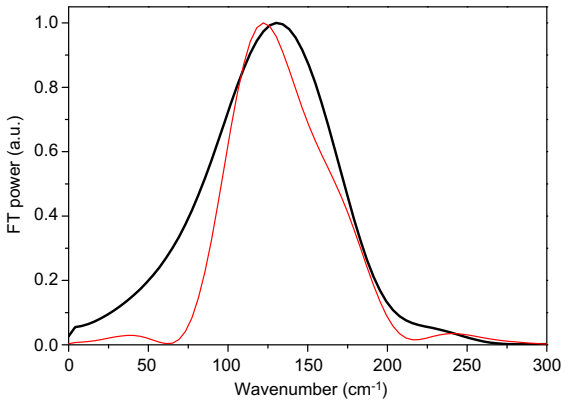

Fig. 4. Fourier power spectra of the gate delay time-dependent traces of the integrated amplitude modulation (AM) (thick line) and frequency modulation (FM) (thin line) shown in Fig. 3.

spectrogram, so that one must pay special attention to this kind of artifact in a spectrogram analysis.

However, it is not the main reason for the modulation observed. A study of the strength of the integrated amplitude modulation has revealed that the amplitude modulation induced by the artifact is much smaller than that of the experiment data. The frequency modulation is also smaller than that observed. Therefore, we can safely conclude that the modulations of neither amplitude nor frequency observed in the present study are mainly caused by the artifact in the calculation but by the interaction between the two relevant modes.

Let us discuss the assignment of the mode with a low modulation frequency. In our previous works, similar phenomena of instantaneous frequency modulation have been observed for bacteriorhodopsin (bR_{568}) and polydiacetylene (PDA) [16,17]. The modulation frequency in bR_{568} was calculated to be 160 cm^{-1} from the Fourier transform calculation, which corresponds to the 200-fs oscillation period of the twist mode around the C=C bond. As for PDA, the frequencies of C=C and C–C stretching are modulated at the vibrational period of the C=C–C bending mode (145 fs) for ~2 ps. In the present Letter, it may be possible to attribute this low-frequency mode to the bending mode in our quinoid–benzenoid polythiophene. This bending mode could be assigned to the C–C=C bending or chain deformation mode [18,19]. The latter deformation mode is considered to involve the out-of-phase translation of adjacent thiophene monomer units. As mentioned in Ref. [18], the frequency of the deformation mode observed in tetrathiophene was reported to be 160 cm^{-1}, and the frequency of this mode was expected to decrease when the number of the thiophene rings increases. Therefore, a candidate of the modulation mode with 120–130 cm^{-1} is the deformation mode with lower frequency than 160 cm^{-1} in the polymer with many more thiophene rings with longer conjugation lengths.

A bending mode is expected to be observed in the real-time traces, so we calculated the FT power of the real-time traces and expanded the frequency below 300 cm^{-1} to show them clearly. As shown in Fig. 2b, a low-frequency located at 114–122 cm^{-1} could be observed at all the wavelengths (marked by the arrows), which are very close to the modulation frequency of 122 and 130 cm^{-1}. This 114–122 cm^{-1} frequency is considered to correspond to 122 or 130 cm^{-1}. Because its oscillation cycle number in the real-time traces is as small as 6, it was difficult to obtain

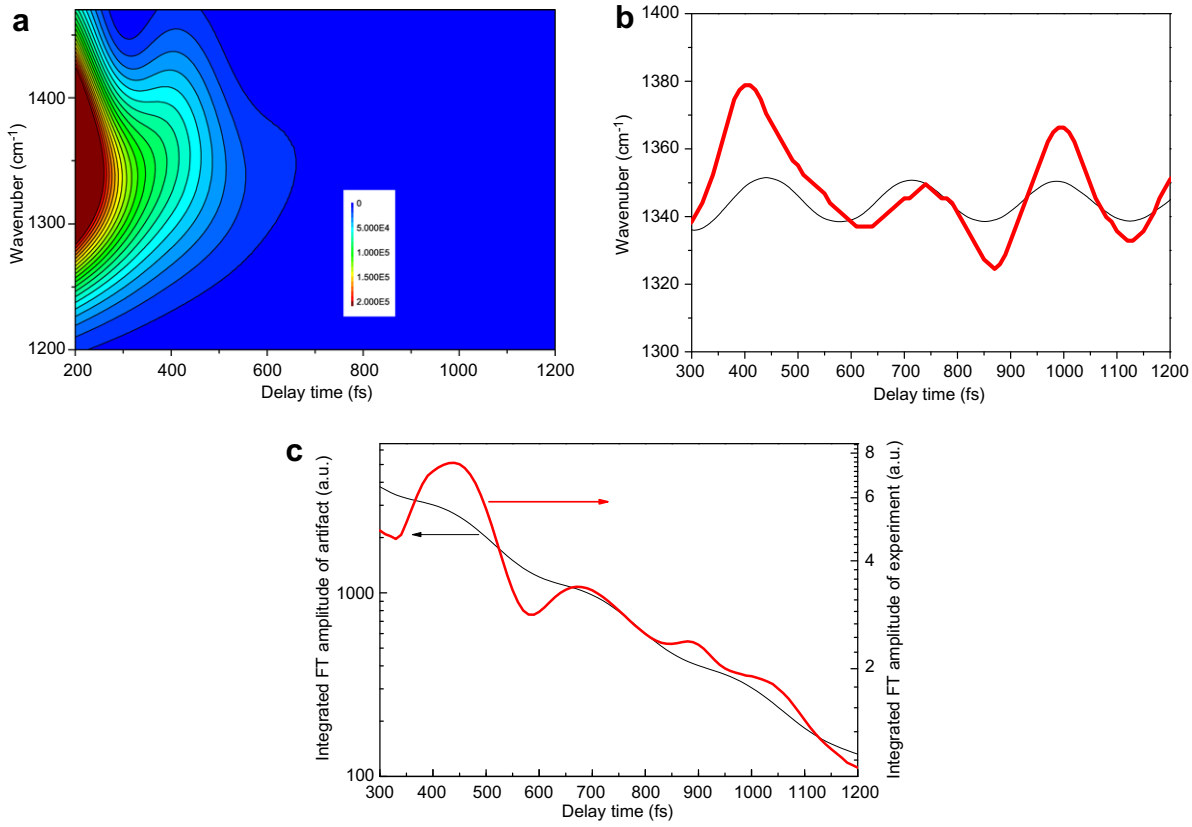

Fig. 5. (a) Contour maps of the spectrograms calculated to show the effect of the artifact using the model of two neighboring modes with the same frequencies as determined experimentally, (b) the instantaneous frequency traces of the simulation for the traces of the artifact (thin line) and the observed (thick line), and (c) the integrated amplitude traces of the artifact (thin line) and the observed (thick line).

its precise frequency, and then it can possibly be attributed to one of the bending modes in the quinoid–benzenoid polythiophene. The mode coupling between the C–C stretching mode and the bending mode is maintained until the vibrational dephasing destroys the coherence of the relevant modes. The decay time of the modulation amplitude due to the mode coupling is longer than 1200 fs, as shown in the spectrogram calculation in Fig. 3.

This finding of frequency and amplitude modulation leads to the conclusion that the bending mode of 120–130 cm^{-1} dynamically couples with the C–C stretching modes through instantaneous bond-order change during the vibration of a low-frequency mode. It means that when the C–C bond with a lower bond order (the center frequency being 1343 cm^{-1}) decreases its order by the flow of a π-electron cloud to the C–C bond with a higher bond order (center frequency being 1465 cm^{-1}), the frequencies of the former and the latter decreases and increases, respectively. In other words, an instantaneous change in the bond order occurs during the bending motion due to the change in the distribution of π-electrons over the relevant C–C bonds.

Another characteristic feature observed in Fig. 3 is the nearly in-phase relation between the amplitude and frequency modulations. The calculated phases of the FM and AM are 0.46π and 0.76π, respectively. The difference between them, 0.30π, indicates the nearly in-phase modulation of AM and FM. Therefore, when the instantaneous frequency is high, the amplitude is large. This may differ from a priori expectation, since the energy belonging to the mode is maintained in the case of opposite behavior, i.e. when the frequency is high the amplitude is reduced. In polydiacetylene, for example, it is found that C=C and C–C stretching modes are coupled through a bending mode and that the instantaneous frequencies of the two stretching modes are anti-correlated [17]. In the present case, the coupling-mediating mode with 120–130 cm^{-1} and/or the mode of 1465 cm^{-1} may increase their instantaneous amplitudes and/or their frequencies to compensate the vibrational energies when that of 1343 cm^{-1} mode decreases. However, it is difficult to define the instantaneous amplitudes and frequencies of these two modes. The high-frequency mode of 1465 cm^{-1} is buried under the robe of the spectrogram distribution of the neighboring mode with 1343 cm^{-1} because the former is much weaker than the latter. The cycle number of the low-frequency (120–130 cm^{-1}) mode in the real-time traces is only 6, which is too small to study the gate delay time dependence of instantaneous frequency and amplitude of this mode.

4. Conclusion

Modulations of both instantaneous vibrational frequency and amplitude have been observed for the C–C stretching mode with the central frequency of 1343 cm^{-1} in a polythiophene thin film. Thus we conclude that a bending mode dynamically couples with the stretching modes through an instantaneous bond-order change during the bending motion. The coupling between the stretching and bending modes is found to be maintained for longer than 1200 fs after photogeneration of the coherent molecular vibration modes. Sufficient attention has been paid to the spectrogram analysis of the real-time traces by taking account of the effect of artifact, which can contribute to the gate delay dependence of both instantaneous vibrational frequency and amplitude because there are two neighboring vibrational modes.

Acknowledgments

The authors are grateful to Profs. Katsumi Yoshino (Shimane Institute for Industrial Technology) and Wei Feng (Tianjin University) for providing us the sample. This work was partly supported by a grant from the Ministry of Education (MOE) in Taiwan under the ATU Program at National Chiao Tung University. A part of this work was performed under the Joint Research Project of the Institute of Laser Engineering, Osaka University, under Contract No. B1-27.

References

[1] F. Garnier, in: K. Müllen, G. Wegner (Eds.), Electronic Materials: The Oligomer Approach, Wiley-VCH, Weheim, 1998, p. 559.
[2] L. Sicot, C. Fiori, A. Lor, J.-M. Nunzi, P. Raimond, C. Sente, Synth. Met. 102 (1999) 991.
[3] O. ganäs, W.R. Salaneck, J.E. Österholm, J. Laakso, Synth. Met. 22 (1988) 395.
[4] M.W. Langeveld-Voss, E. Peeters, R.A.J. Janssen, E.W. Meijer, Synth. Met. 84 (1997) 611.
[5] D.D.V. Rughooputh, S. Hotta, A.J. Heeger, F. Wudl, Polym. Phys. 25 (1987) 1071.
[6] K. Yosho, S. Nakajima, D.H. Park, R. Sugimoto, Jpn. J. Appl. Phys. 27 (1988) L716.
[7] K. Yosho, P. Love, M. Onoda, R. Sugimoto, Jpn. J. Appl. Phys. 27 (1988) L2388.
[8] G. Harrison, R.H. Friend, in: K. Müllen, G. Wegner (Eds.), Electronic Materials: The Oligomer Approach, Wiley-VCH, Weheim, 1998, p. 515.
[9] V. Marta, K. Ionescu, L. Pigani, F. Terzi, A. Ulrici, C. Zanardi, R. Seeber, Anal. Bioanal. Chem. 387 (2007) 2101.
[10] W.C. Chen, S.A. Jenekhe, Macromol. Chem. Phys. 199 (1998) 655.
[11] W. Feng, W.H. Yi, H.C. Wu, M. Ozaki, K. Yosho, J. Appl. Phys. 98 (2005) 034301.
[12] T. Kobayashi, J. Du, W. Feng, K. Yoshino, Phys. Rev. Lett. 101 (2008) 037402.
[13] A. Shirakawa, T. Kobayashi, Appl. Phys. Lett. 72 (1998) 147.
[14] A. Shirakawa, I. Sakane, T. Kobayashi, Opt. Lett. 23 (1998) 1292.
[15] A. Baltuška, T. Fuji, T. Kobayashi, Opt. Lett. 27 (2002) 306.
[16] T. Kobayashi, T. Saito, H. Ohtani, Nature (London) 414 (2001) 531.
[17] T. Kobayashi, A. Shirakawa, H. Matsuzawa, H. Nakanishi, Chem. Phys. Lett. 321 (2000) 285.
[18] D. Birnbaum, D. Fichou, B.E. Kohler, J. Chem. Phys. 96 (1991) 165.
[19] E. Faulques, W. Wallnöfer, H. Kuzmany, J. Chem. Phys. 90 (1989) 7585.